Journal of Structural Geology 32 (2010) 1721–1731

Contents lists available at ScienceDirect

Journal of Structural Geology

journal homepage: www.elsevier.com/locate/jsg

# Field evidences for the role of static friction on fracture orientation in extensional relays along strike-slip faults: Comparison with photoelasticity and 3-D numerical modeling

Roger Soliva [a,*], Frantz Maerten [a,b], Jean-Pierre Petit [a], Vincent Auzias [c]

[a] Université Montpellier II, Lab. Géosciences Montpellier, UMR 5243, Place E. Bataillon, 34095 Montpellier cedex, France
[b] IGEOSS, Parc Euromédecine, 340 rue Louis Pasteur, 34790 Grabels, France
[c] BERKINE SONATRACH ANADARKO, Rte de Cina, 16001 Hassi Messaoud, Algeria

ARTICLE INFO

*Article history:*
Received 25 May 2009
Received in revised form
14 January 2010
Accepted 18 January 2010
Available online 28 January 2010

"To the memory of Maurice Mattauer, professor at the University of Montpellier II, who left us in April 2009"

*Keywords:*
Fault
Friction
Relay
Wing cracks
Damage zone

ABSTRACT

Fault friction is a parameter that is difficult to assess along fault zones since its determination depends on the knowledge of any factor controlling the state of stress around faults. In brittle homogeneous rocks, a limited number of these factors, such as the shape of the fault surface, the vicinity of fault tips or the remote stress ratio, are crucial to constrain for this determination. In this paper, we propose to analyse a field example in which all these properties are met and where the nature of the slipped structure suggest differences in static friction. We compare the orientations of branching fractures at strike-slip relay zones between en echelon stylolites and en echelon joints both reactivated in shear. The field data are compared with both photoelastic and 3-D numerical models that consider the remote stress conditions and the role of the geometry of the strike-slip segments. Based on field observations, these analyses quantitatively demonstrate the significant role of fault friction on the local stress field orientation and subsequent fracture formation. This work points out that estimations of fault friction based on analyses of fracture patterns or in situ stresses must be accompanied with a thorough investigation of the 3-D fault shape, its segmentation and the remote stress state.



## 1. Introduction

Static friction along faults is an extremely important parameter for the understanding of the seismic cycle, the distribution of stresses, fracture patterns and damage zones around faults. In the past decades many efforts have been made to estimate fault friction along natural faults (e.g. Hanks, 1977; Zoback and Zoback, 1980; Brace and Kohlstedt, 1980; Lachenbruch and Sass, 1980; Zoback and Healy, 1984; Mount and Suppe, 1987; Brudy et al., 1997; Zoback et al., 1987; Scholz, 2000). The measure of static friction estimated using laboratory tests on fault gouges is scale-limited, i.e. on gouge samples from a bore hole cutting crossing the fault, and therefore may not represent the frictional state of the whole surface. Other approaches, based on the analyses of the heat flow (Brune et al., 1969; Lachenbruch and Sass, 1980; d'Alessio et al., 2003) or numerical modeling (e.g. Parsons, 2002; Lovely et al., 2009), allow discussion on the state of friction along the fault but are quite indirect. The analysis of in situ stresses from bore hole measurements or fracture patterns are considered as the best indicator of the frictional state along a fault, (Zoback and Healy, 1984; Zoback et al., 1987; Scholz, 2000).

Assuming that fault cohesion can be close to zero on an active fault (Byerlee, 1978), the static friction has been approximated by Amonton's first law, in which the frictional cœfficient ($\mu$) is expressed as a function of the shear ($F$) and normal ($N$) components of the forces applied to a frictional surface.

$$F = \mu^{*}N \tag{1}$$

This law states that the friction coefficient of an infinitely long fault surface is directly related to the orientation and the magnitude of the stresses close to this surface (Fig. 1a). This reveals that the analysis of the stress field around a fault can be used to determine the static friction along a fault, in cases where the remote ratio of stresses applied to the sliding surface is known. Therefore, any indicators of the stress field around faults

* Corresponding author.
*E-mail addresses:* roger.soliva@gm.univ-montp2.fr (R. Soliva), fmaerten@igeoss.com (F. Maerten), vincent_auzias@berkine.com (V. Auzias).

0191-8141/$ – see front matter © 2010 Elsevier Ltd. All rights reserved.
doi:10.1016/j.jsg.2010.01.008

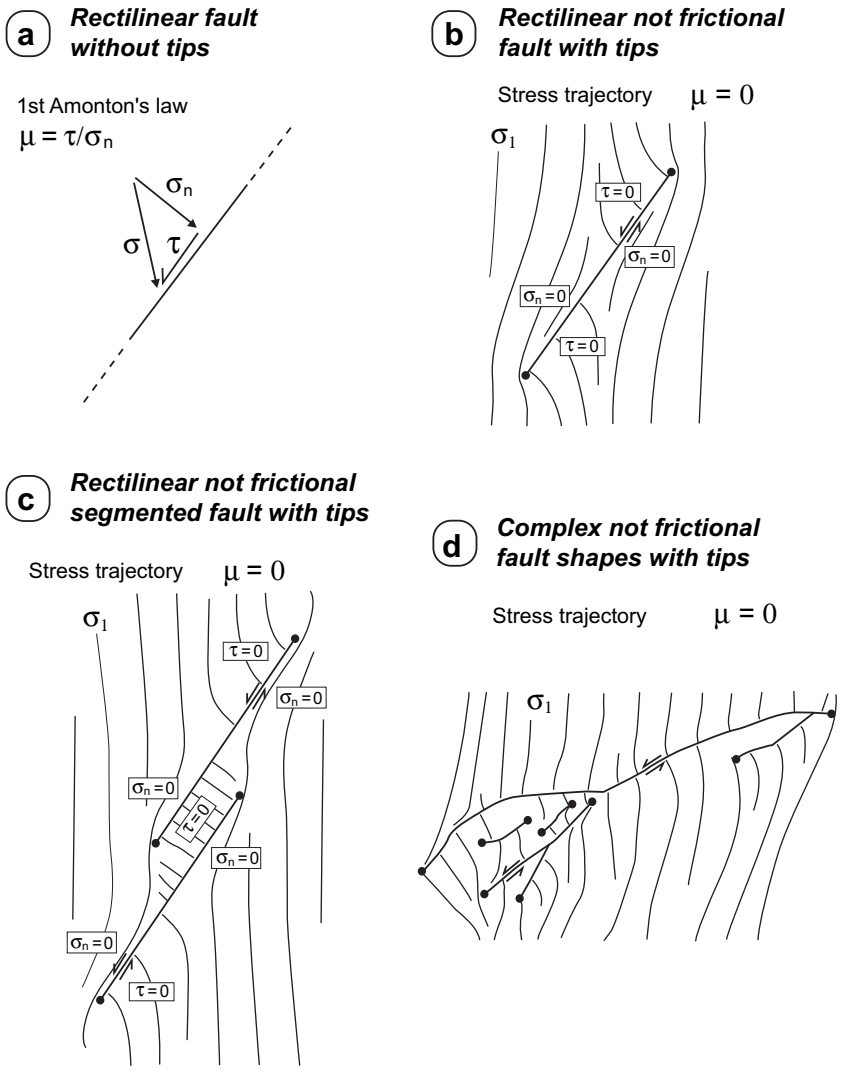


**Fig. 1.** Comparison between the stress perturbation due to fault friction (a) and the stress perturbation due to different examples of fault geometry (b, c and d). (b), (c) and (d) are $\sigma_1$ stress patterns inferred from photoelastic modeling (Joussineau et al., 2003). The remote stress applied is uniaxial. Dots represent fault tips. This figure shows that even for $\mu = 0$, the orientation of $\sigma_1$ can be oblique and even parallel to the fault surface, rather than perpendicular as suggested by Amonton's first Law.

(e.g. bore hole analysis, faults or fracture patterns) provide the opportunity to quantify the static friction. However, this analytical approach, based on Amonton's first law, assumes that the fault plane is rectilinear and that the fault tips are infinitely far from the study area. Such a first order approximation is quite unrealistic for natural faults having tips, being irregular, segmented or more complex in shape (Fig. 1b–d). The local orientation and magnitude of the stress field around a fault does not rely only on fault friction, which makes its determination non-unique unless we have knowledge of the other factors perturbing the local stress field.

In homogeneous rocks, the first parameter that has been considered as acting on the local stress field, and more precisely on the crack angle to a fault, is the static friction coefficient (e.g. Petit and Barquins, 1988; Barquins et al., 1997; Martel, 1997; Ohlmacher and Aydin, 1997; Willemse and Pollard, 1998; Zhou, 2006; Mutlu and Pollard, 2008). However, the remote stress angle has been considered as very important (Barquins et al., 1992; Ohlmacher and Aydin, 1997) as well as the remote stress ratio (Auzias et al., 1997; Katternhorn et al., 2000; Zhou, 2006). Others factors more related to the geometry and behaviour of the fault surface also seem to be very influential, as the 3-D geometry of the faults (e.g. Segall and Pollard, 1980; King et al., 1994; Willemse, 1997; Maerten et al., 2002; Bourne and Willemse, 2001), its spatial/temporal evolution (Willson et al., 2007; Lunn et al., 2008; Moir et al., 2009), and fault opening (Kattenhorn and Marshall, 2006). Therefore, any analysis of fault zones that aims to estimate the role of fault friction on the stress field, or in contrast to determine the state of friction from stresses analysis, must know any of these factors that can perturb the local stress field.

In this paper, we analyse a field example in which these factors can be estimated. Drastic differences in fracture orientation between reactivated frictional stylolites (i.e. structures of high friction coefficient) and frictionless joints (i.e. structures of low friction coefficient) suggest that friction is a prominent property influencing the stress perturbation at the close vicinity of a fault. We chose to study fracture orientation at extensional relay zones because the stress orientation has been described as quite stable in space along a relay zone (compared to outside) due to the juxtaposition of the two extensive fault quadrants (see Fig. 1c) (e.g. Auzias et al., 1997; Ohlmacher and Aydin, 1997). We compare the field data to photoelastic and 3-D numerical models to demonstrate and quantify the significant role of static friction on the stress and fracture orientation at extensional relay zones.

## 2. Field data

### 2.1. Geological setting

The studied exposure, located close to Les Matelles (15 km North of Montpellier, France, Fig. 2), is a suitable site for the study of brittle tectonics in limestones and stress perturbations around meso-scale faults (Rispoli, 1981; Fletcher and Pollard, 1981; Petit et al., 1999). The brittle tectonic structures observed (Fig. 3a) were formed during multiphase compressive tectonics allowing the formation of joints and stylolites. These structures of similar dimension and orientation have been reactivated as slip surfaces during a late tectonic event (Petit and Mattauer, 1995). Because of their different roughness, joints and stylolites are expected to be of different frictional properties during slip. Most of them show secondary fracturing and linkage at relay zones (Fig. 3b), that can be used as indicators of the palaeostress orientation (e.g. Rispoli et al., 1981; Petit and Mattauer, 1995). It is therefore worthwhile to address with particular care on the geological setting and history of the brittle structures that will be used to constrain the role of fault friction on fracture orientation.

The studied exposure has been fully described in a number of previous studies (e.g. Rispoli et al., 1981; Taha, 1986; Petit and Mattauer, 1995; Petit et al., 1999). This area is located in the vicinity of a fault branch called the Lirou fault (Fig. 2b). The Matelles fault zone, like many faults in the area, had both left-lateral strike slip related to the Pyrenean shortening and normal slip related to the Oligocene rift extension in the Languedoc. Middle cretaceous normal slip along the Matelles–Corconne fault zone is also expected during the Durancian tectonic events.

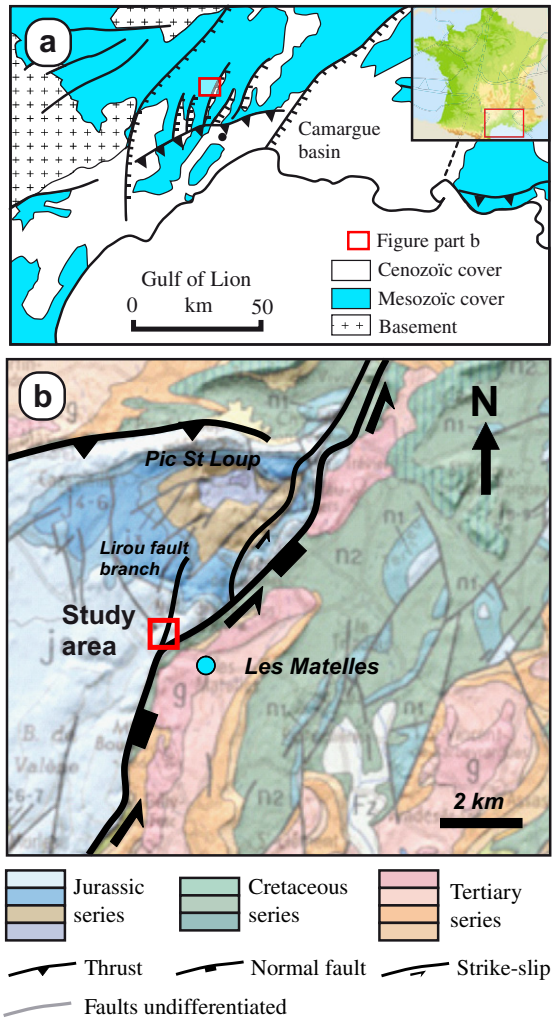


**Fig. 2.** Location and geological context of the study area. (a) Structural scheme of the study area. (b) Geological map of the study area showing the Matelles fault and the Lirou fault branch, modified from the geological map of St Martin de Londres, 1/50,000.

The brittle deformation sequence described by Petit and Mattauer (1995) begins by a vertical jointing stage of the limestone layers with two principal trends, N020 and N140. The second stage is a first generation of stylolite formation oriented N040. The third stage, the most important for our study, is the reactivation of the previous structures as sinistral and dextral strike slips due to a last shortening creating wing cracks, en echelon veins and a second generation of stylolites around the reactivated defects. As shown by this last generation of joints and stylolites formed, the last shortening stage occurs with the maximum principal stress ($\sigma_1$) oriented North–South. As suggested by rock experiments, photoelastic models, numerical and analytical solutions (see Wawersik and Brace, 1971; Petit and Barquins, 1988; Barquins and Petit, 1992; Chaker and Barquins, 1996; Lunn et al., 2008) the presence of wing cracking around reactivated defects (see Fig. 3b) implies remote stress conditions close to uniaxial loading ($\sigma_1/\sigma_3 \geq 10$). Conditions close to horizontal uniaxial stresses are possible at shallow depths, i.e. for little confining pressure. The expected depth of faulting in the upper Jurassic limestone was probably less than the thickness of the lower cretaceous series ($\sim$200 m), which was potentially yet well eroded during the Pyrenean shortening. This local stress state condition (high ratio of maximum to minimum principal stresses, $\sigma_H/\sigma_h$) and reorientation of $\sigma_1$ axis has been related to a restraining bend along the *Les Matelles fault* during Pyrenean strike-slip movements (Rawnsley et al., 1992; Petit et al., 1999).

### 2.2. Extensional relay geometries

The last stage event provides the opportunity to analyse the geometry of branching at relay zones between slipped overlapping stylolites vs. slipped overlapping joints (Figs. 4 and 5a). The angle $\beta$, defined as the angle between the orientation of remote $\sigma_1$ relative to the joints or stylolites reactivated in shear (Fig. 5c), is quite variable (variation of $\sim 40^\circ$). A wide overlap of $\beta$ angles is therefore found for reactivated joints and stylolites containing relay zones. For similar $\beta$ angles, the branching angle $\alpha$ (defined as the angle between the slipped structure and the branching jog) is quite different with respect to the nature of the reactivated structure. More precisely, for similar $\beta$ angles, $\alpha$ is larger for joints than stylolites (Fig. 5a and b). These observations are verified on a $\alpha$ vs. $\beta$ graph, in which additional measures from the literature were reported for comparison. Field data from stylolites and joints are consistent with the general scatter of all the data, and fit in two specific fields of branching configurations as described above. Because of their different roughness (see Delair and Leroux, 1978; Raynaud and Carrio-Schaffhauser, 1992, for the analysis of non-reactivated stylolites), joints and stylolites are expected to be of different frictional properties during slip. Therefore, the question arising from these observations and treated in the next sections is the following: Is this difference of branching geometry really due to the frictional properties of the slipped structures? The local orientation of relay branching fractures ($\alpha$) gives a good approximation of the local orientation of $\sigma_1$ during fault slip of all the faults measured and at the same tectonic event (e.g. Auzias, 1995; Ohlmacher and Aydin, 1997; Kattenhorn et al., 2000). The wide range of $\alpha$ angle observed in the field therefore reveals wide variation in the ratio of shear stress/normal stress, probably due to

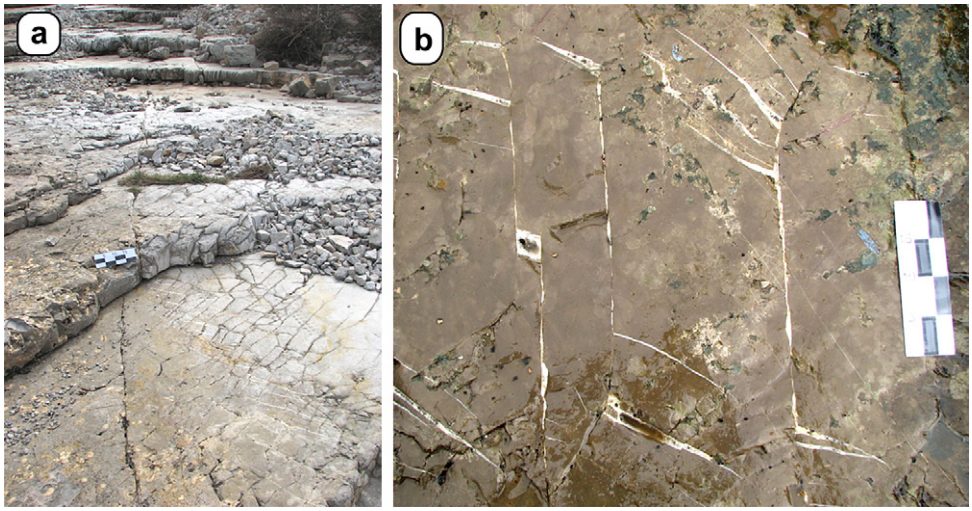


**Fig. 3.** Field photographs of the study area. (a) Outcrop overview showing the layered upper Jurassic mudstones damaged by a dense pattern of calcite sealed fractures and stylolites. (b) First generation stylolites reactivated as sinistral strike slips showing wing cracks and branched stylolites (see Rispoli, 1981). The length of the scale bar is 20 cm.

variations in static friction of the slipped structures. This hypothesis will be tested below using analogue and numerical modeling.

## 3. Photoelastic modeling

### 3.1. Photoelastic method

A way to test the effect of friction is to analyse the stress field orientation using photoelastic experiments around opened (not frictional, i.e. $\mu = 0$) and closed defects (frictional). Photoelasticity is an optical method of stress analysis within elastic translucent materials like polymethylmethacrylate (PMMA), which present accidental birefringence when loaded. These materials have the property of resolving the light which falls on them at normal incidence into two components, each one coinciding with a principal plane of stress. This property, due to a higher density of the material in these stress orientations, implies a light transmitted at right angles (Hetényi, 1966). If a photoelastic sample is placed between crossed polarizers, black fringes named isoclinics (light extincted, see Fig. 6b for an example) are observed on the second polarizer, i.e. the analyzer. Isoclinics correspond to locations where the plane of the incident polarized light coincides with one direction of principal stress within the sample. These isoclinics move when the polarizers rotate together. By rotating the polarizers from 0° to 90°, and drawing the corresponding isoclinics, it is possible to map the orientation of the two principal stresses. A thorough description of the same experimental device (Fig. 6a) and additional details about the photoelasticity method can be found in Joussineau et al. (2003).

To simulate the effect of fault friction on the stress field of extensional relay zone, two types of PMMA models were compared: a first one composed of closed defects and assumed to have friction, and the other one with opened defects and assumed to have negligible friction. To produce open defects, the thin plates of PMMA (0.5 cm thick, 6.5 cm width and 10 cm high) were sawn-off with a 300 μm thick micro-saw from central drill holes on each interacting segments of 500 μm diameter. Closed defects were produced as planar fractures propagated along linear traces drawn with a cutter on the PMMA surface. These two types of models are subjected to loading with different $\beta$ angle such as 20°, 45° and 70°. Here $\beta$ is the angle between the axial loading and the planar defects forming the relay zone.

The models are subjected to uniaxial conditions in order to be consistent with the field conditions expected (see Section 2). The axial compressive load is imposed by an electromechanic testing machine (Davenport 30 kN) and no lateral pressure is added. To prevent bending of the PMMA plate under vertical loading, the samples are maintained between vertical tighteners.

### 3.2. Experimental results of extensional relay stress pattern

The two types of models (frictional vs. not frictional) show significant differences in their local stress field distribution. Fig. 7 presents stream lines of $\sigma_1$ for not frictional (a) and frictional configuration (b) subjected to a vertical loading with $\beta = 20°$. The stress field is less perturbed in orientation for the frictional case. Without friction, the orientation of $\sigma_1$ is normal to the faults (deviation of 70° from the remote $\sigma_1$) and quite stable along the relay zone. Also note that the stress field is perturbed outside of the relay zone. In the frictional case, the stress field changes from the tip, where it is close to vertical, to the center of the relay zone, where it reaches its maximum deviation of 45°. Additional tests, not presented here and done for variable overlap and constant spacing between the defects, show the same maximum values of $\sigma_1$ deviation and a better stability of $\sigma_1$ orientation in the relay zone as the overlap increases.

All the studied tests show results generally consistent with field observations. Fig. 8 exhibits the compilation of the $\alpha$ and $\beta$ angles data for all the tests done with constant relay geometry. Note that $\alpha$ here corresponds to the angle between the slipped defect and $\sigma_1$ at the center of the relay zone. Tests with no friction lie in the graph area of high $\alpha$ and relatively low $\beta$ angles, which corresponds to the zone of slipped joints (of low friction compared to slipped stylolites). In contrast, frictional tests data lie in the area of lower $\alpha$ and relatively high $\beta$ angles, which corresponds to the zones of slipped stylolites (high friction).

## 4. Numerical modeling

The numerical code used to investigate fault friction is a 3-D Boundary Element Method (BEM) called Poly3D (Thomas, 1993). It relies on the analytical solution of an angular dislocation in a homogeneous elastic whole- or half-space (Comninou and Dundurs, 1975). As opposed to the Okada's code (Okada, 1985),

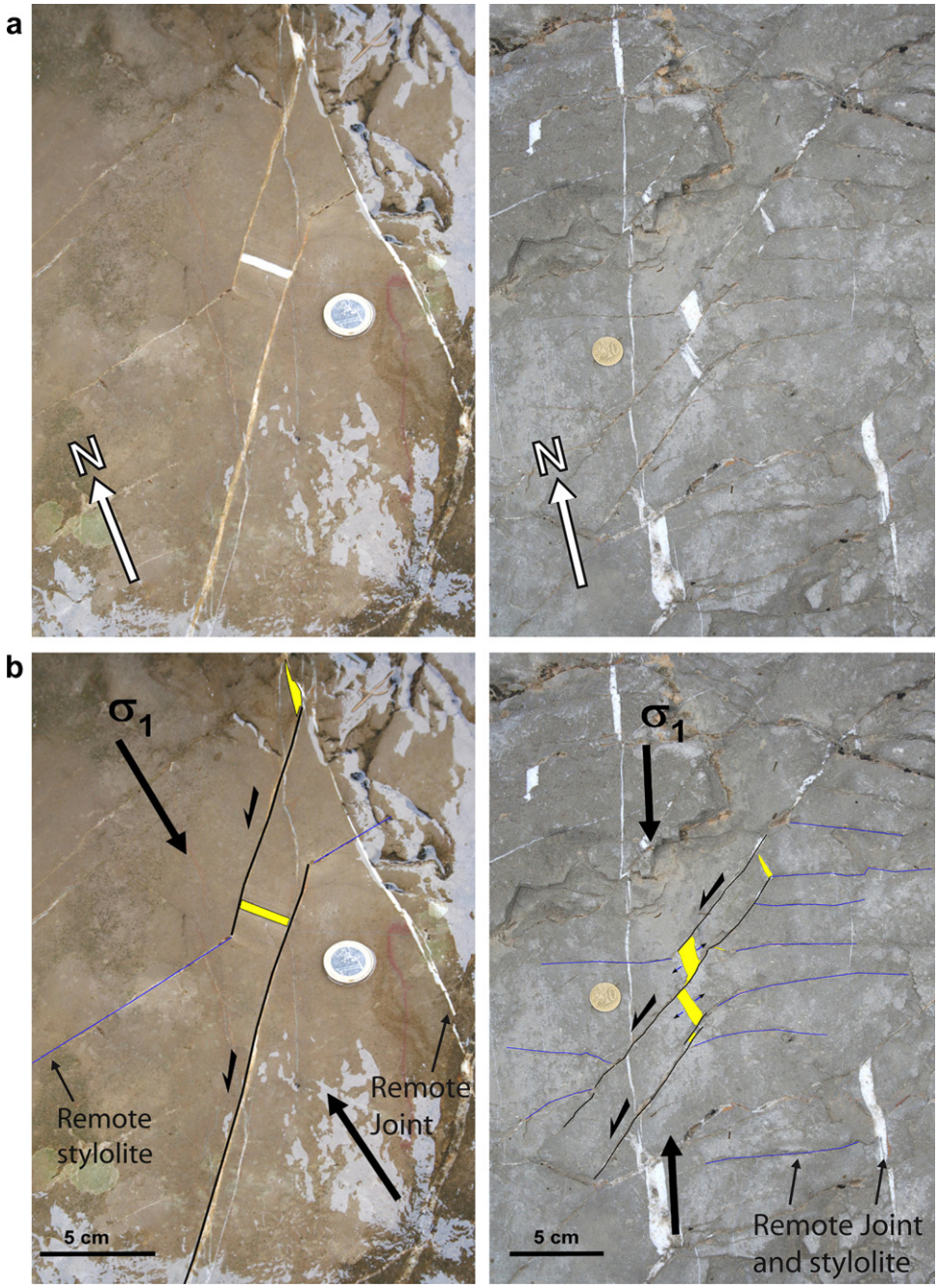


**Fig. 4.** (a) Examples of joints (left side) and stylolites (right side) reactivated as left-lateral strike slips. (b) Interpretation in terms of stress orientation using the remote orientation of syn-kinematic joints and stylolites. The "remote stress" orientation is slightly different in the two cases because they were not measured at the same location and that the larger Lirou fault probably modify the stress field orientation at this North–South last compressive stage.

which uses rectangular elements, Poly3D discretizes faults and fractures using triangular elements, and therefore avoids the creation of overlaps and gaps between adjacent elements which perturb the solution (Maerten et al., 2005). Mixed traction–displacement boundary conditions can be used for each constitutive element of the model (tractions are shear and normal stresses resolved on the fault surface). When traction boundary conditions are specified, we have to solve for the corresponding unknown displacement discontinuity according to the initially prescribed traction values. As soon as all displacement discontinuities are known (i.e. the slip patches), strain, stress and displacement can be computed at any observation point within the elastic field. Note that transient variations in friction coefficient or the dynamic stress field are not considered (e.g., Poliakov et al., 2002).

In order to have a frictional behaviour, the code has been extended to support inequality constraints on traction and displacement. Specifically, the static Coulomb friction has been implemented as a traction inequality constraint and validated by comparison with analytical and numerical solutions (Maerten et al., 2009). For a given fault surface, the coefficient of friction and cohesion can be prescribed globally onto a fault surface or locally, each constitutive element having their own coefficients. Traction boundary conditions are imposed along the three axis of each triangular element local coordinate system (dip, strike and normal directions).

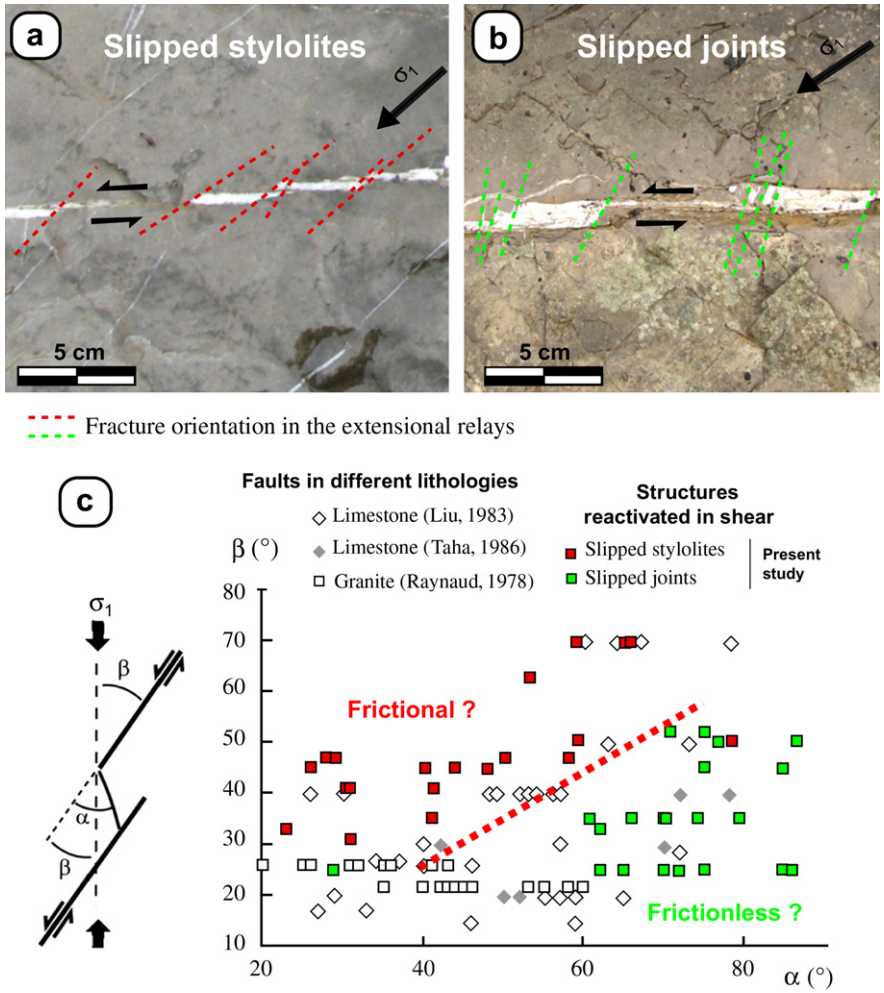


**Fig. 5.** Variation in the geometry of extensional jogs between stylolites and joints reactivated in shear. (a) and (b) are field examples of reactivated stylolites and joints, respectively. Coloured dashed lines represent the orientation of fractures in the relay zones. (c) Graph of $\alpha$ and $\beta$ angles for all the reactivated stylolites and joints measured in the field. $\alpha$ and $\beta$ angles are represented in a small scheme at the left. Field observations show higher $\beta$ angles for reactivated stylolites.

For a model subjected to a compressive far field stress, interpenetration of the elements has to be avoided. This is achieved by using the displacement inequality constraint $u_z \geq 0$, where $u_z$ represents the computed normal displacement of a triangular element. Again, traction boundary conditions are imposed along the three axes of each triangular element local coordinate system (Maerten et al., 2009).

### 4.1. Model set up

Fig. 9a and b depicts the model configurations used for the BEM modeling for joints and stylolites, respectively, and are built upon field observations (Fig. 4). All the veins and stylolites traces in the vicinity of the zone of interest have been carefully mapped and then vertically extruded in depth all along the limestone layer thickness, giving rise to the 3-D triangulated surfaces. As the Coulomb friction relates the shear to the normal components of the forces applied to a frictional surface, traction boundary condition for the three local axes (dip, strike and normal) of each constitutive triangular element is used.

### 4.2. Modeling of joints reactivated in shear

The joints model, depicted in Fig. 9a, is based on the field observations shown in Fig. 4, left side. These first generation joints are subjected to a far field remote stress with uniaxial compressive condition and $\sigma_1$ (in this area) oriented N170 as suggested by the presence of surrounding joints and stylolites (third brittle deformation stage, see Section 2). In order to display the stress orientation within the extensional relay resulting from the computed displacement discontinuities, an observation grid is placed close to the top of the model (Fig. 9). Then, two simulations are performed: a first one, with a constant coefficient of friction $\mu = 0.6$ for all discontinuities and no cohesion, and a second without any friction but with "non-interpenetration" as a unique constraint. The elastic material properties used for the surrounding limestone are $\nu = 0.25$ and $E = 1$ GPa (see Hatheway and Kiersch, 1989).

Fig. 10a and b displays the frictional and not frictional models, respectively. The orientation of $\sigma_1$ axis fit better with the strike of the branching fracture in the case where the frictional coefficient equals zero. Since $\sigma_1$ should be parallel to the strike of the branching fracture, these models suggest that, at the initiation of the linkage, the slipping joints were preferably not frictional. This is consistent with the absence of macroscopic irregularities along these rectilinear structures.

### 4.3. Modeling of stylolite reactivated in shear

For the stylolites model depicted in Fig. 9b, the uniaxial compressive far field stress is oriented N015, as proved by the

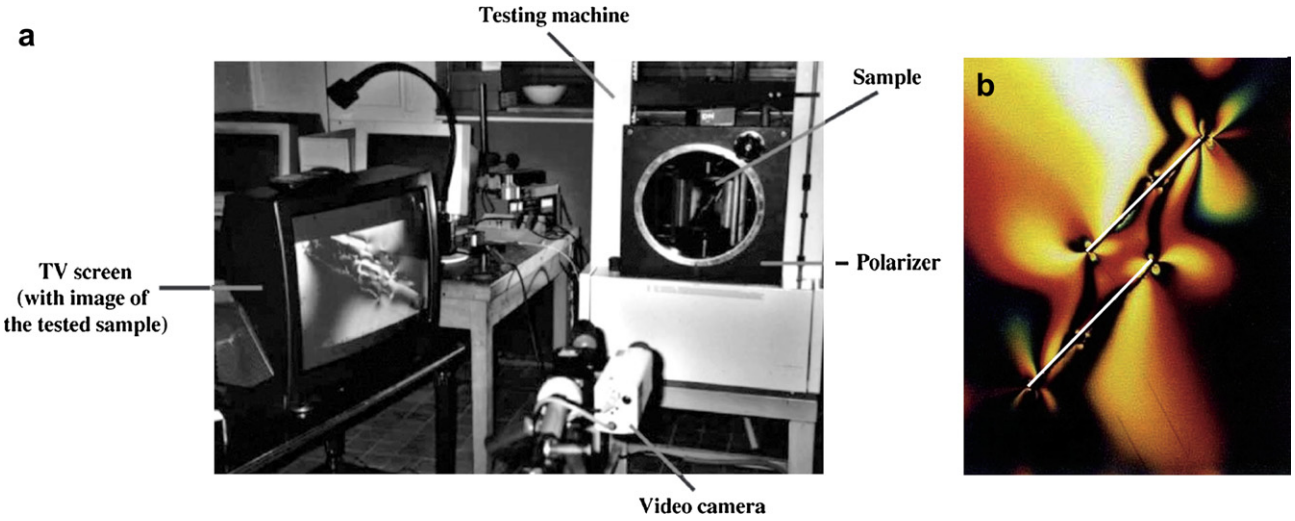


**Fig. 6.** (a) Experimental device of the photoelastic modeling. (b) Example of isoclinic and isochromic fringes obtained in a vertical uniaxial loading experiment of slipping overlapping open defects.

presence of surrounding joints and stylolites (see Fig. 4, right hand side, and Fig. 9b in Petit and Mattauer, 1995). Since this model is composed of two relays, two observation grids are placed in the vicinity of them close to the top of the model. A first simulation is done using only the non-interpenetration constraint (i.e. with $\mu = 0$), whereas a second one employs a constant coefficient of friction $\mu = 0.6$ without cohesion.

Fig. 11a and b displays the results on the two observation grids for the not frictional and frictional models, respectively. As opposed to the previous joint modeling, the linking structures are more consistent with high friction stress orientations.

### 4.4. Parametric analysis

A series of models have been done for variable friction and constant fault geometry consistent with the overlapping segments of the experimental PMMA model. The 3-D shape of the model is shown in Fig. 12a. The results are analyzed on the observation grid which allows to compare a configuration close to the field and the photoelastic modeling (Fig. 12b). The models were performed with variation of static friction coefficient and $\beta$ angles as shown in Fig. 12c. The elastic material properties used are the same than above since a large part of the field data used for comparison were measured in limestone (Fig. 5).

The results are in good agreement both with field and experimental data. Fig. 13 exhibits the compilation of the $\alpha$ and $\beta$ angles data for all the tests done. As for the experimental analysis, $\alpha$ corresponds to the angle between the slipped surface and $\sigma_1$ at the center of the relay zone. The numerical models with no or little friction lay in the graph area of high $\alpha$ and relatively low $\beta$ angles, which corresponds to the zone of slipped joints (frictionless structures). In contrast, frictional models fit in the area of low $\alpha$ and relatively high $\beta$ angles, which corresponds to the zone of slipped stylolites (frictional structures).

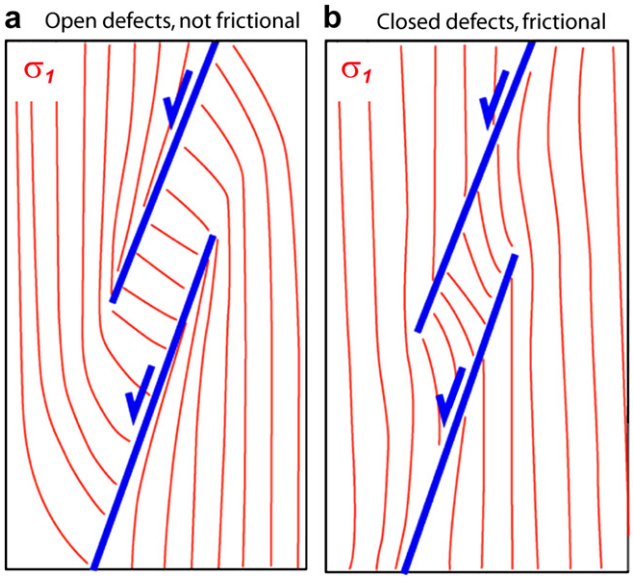


**Fig. 7.** Drawing of $\sigma_1$ obtained from the analysis of isoclinic fringes for (a) uniaxial vertical loading of open defects, i.e. non-frictional and (b) closed defects, i.e. frictional.

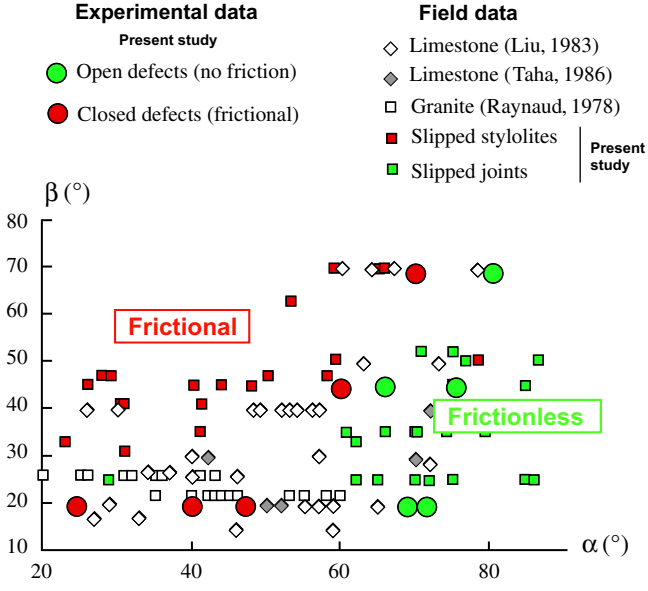


**Fig. 8.** Comparison between $\alpha$ and $\beta$ angles obtained by photoelastic modeling with the dataset measured in the field.

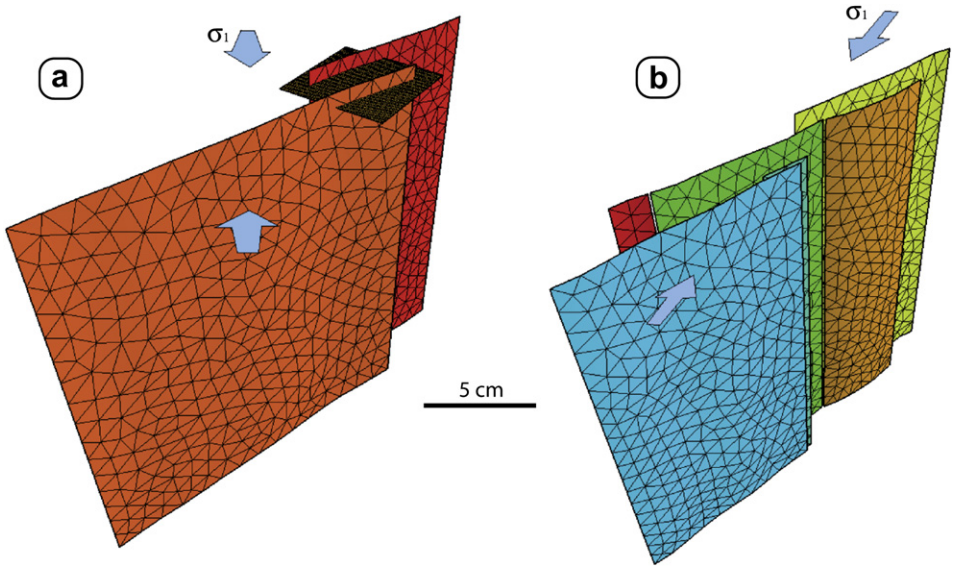


**Fig. 9.** 3-D view of the geometry of the defects reactivated in shear used in Poly3D for the numerical simulation. (a) 3-D geometry of the reactivated joints shown in Fig. 4 with the observation grid (dark square) on which the stresses are represented in Fig. 10. The position of the observation grid corresponds to the position of the top of the limestone layer observed in the field. (b) 3-D geometry of the reactivated stylolites shown in Fig. 4. The observation grids (not shown here), on which the stress field is presented in Fig. 11, are placed at the same level than in (a).

## 5. Discussion

### 5.1. Stress perturbation and friction of the slipping defects

The models are in good agreement with the field observations, however they do not cover the entire range of data, especially for the low $\alpha$ angles (Fig. 13). This point can be discussed with respect to a limited number of unconstrained factors that may influence the stress field around the slipping defects.

Inelastic deformations can modify the magnitude of residual stresses in the host rock around faults, but this is probably not the explanation of the scatter observed in Fig. 13 for two reasons. First, with respect to the brittle subsurface conditions of deformation, the studied limestone probably has negligible inelastic behaviour preceding its shear yielding strength (Rispoli, 1981; Petit and Mattauer, 1995). Second, inelastic deformation around fault, if any, has probably a larger influence on the stress magnitude than on the orientation (Bürgmann and Pollard, 1994), which one close to the fault must be directly related to fault friction. This suggests that elastic models are relevant to simulate residual stresses related to fault slip in this geological context, and that the spreading of field data compared to the model is mainly due to others factors.

The effect of 3-D fault geometry, especially the fault aspect ratio, on the stress distribution around fault has probably little influence. Soliva et al. (2006) show that the dimension of the area of stress perturbation around a fault scales linearly with the fault length since the fault growth is radial, and tends to be limited to a certain distance when the fault height reaches a constant value. This means that for vertically restricted fault by strata bounds, the 3-D shape can influence the orientation of the stress field at about a distance around the fault equivalent to the layer thickness. In the present study, for all the measures of angles made in the field (in the relay zones), the distance of the fractures around the faults is always lower than the layer thickness potentially restricting the faults (tens of cm). We therefore work in a window around the faults where the stress perturbation should not be influenced by the fault aspect ratio (3-D shape), and that all the field measurements could be compared to 2-D photoelastic models or 3-D full space models proposed.

The reason of the difference of scatter between the field data and the models is potentially purely geometric. For all the model results presented in Fig. 13 (both parametric and photoelastic), the fault configurations are idealized as two planar surfaces with constant overlap and spacing, whereas the field data are from faults more complex in shapes, with variable overlap and spacing, curved, with multiple segments and potentially more complex in 3-D.

We have shown that friction is the main factor controlling the stress perturbation and the orientation of linking fractures. However the physical cause for this variation in friction needs to be discussed. Obviously, this cause can be reasonably ascribed to the difference of surface roughness between the stylolites and the joints. However, the analysis of the roughness of the slipped defects is not very relevant on faulted stylolites since after faulting they show a smoothed irregularity that is certainly different than the initial one. The measure of roughness has been done on non-reactivated stylolites (see Delair and Leroux, 1978; Raynaud and Carrio-Schaffhauser, 1992, for the quantitative analysis of stylolites roughness in the same study area). However, these stylolites were not reactivated potentially because of a threshold friction, then different than the initial state on the faulted stylolites. On the other hand, efforts in measuring the surface roughness of the slipped defects cannot be very conclusive since it represents the finite strain.

### 5.2. Estimation of fault friction and upscaling

From three different approaches: (1) field study, (2) experimental modeling and (3) numerical modeling, we have shown that the angle of fracture branching in strike-slip relay zones is highly dependent on the frictional state of the overlapping faults.

It is worthwhile to note that the "static" friction estimated at the relay zone corresponds to the friction of the faults in the vicinity of the relay zone and at the time of the fault interaction through the relay zone. This frictional property may therefore have evolved through time and space with the progression of fault coalescence. The "quasi-static" friction estimated must be therefore considered as the time integrated friction of the period of fault interaction through their stress field. We also must keep in mind that this

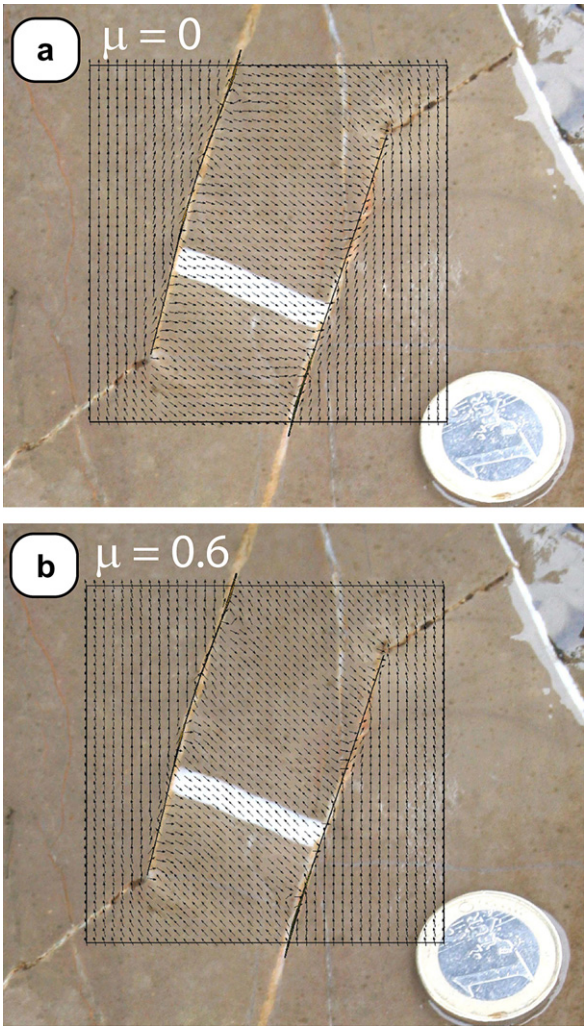


**Fig. 10.** Model results for the joints reactivated in shear shown in Fig. 9. (a) Modeling result for $\mu = 0$. (b) Modeling result for $\mu = 0.6$. The small arrows on the observation grid show the local orientation of $\sigma_1$.

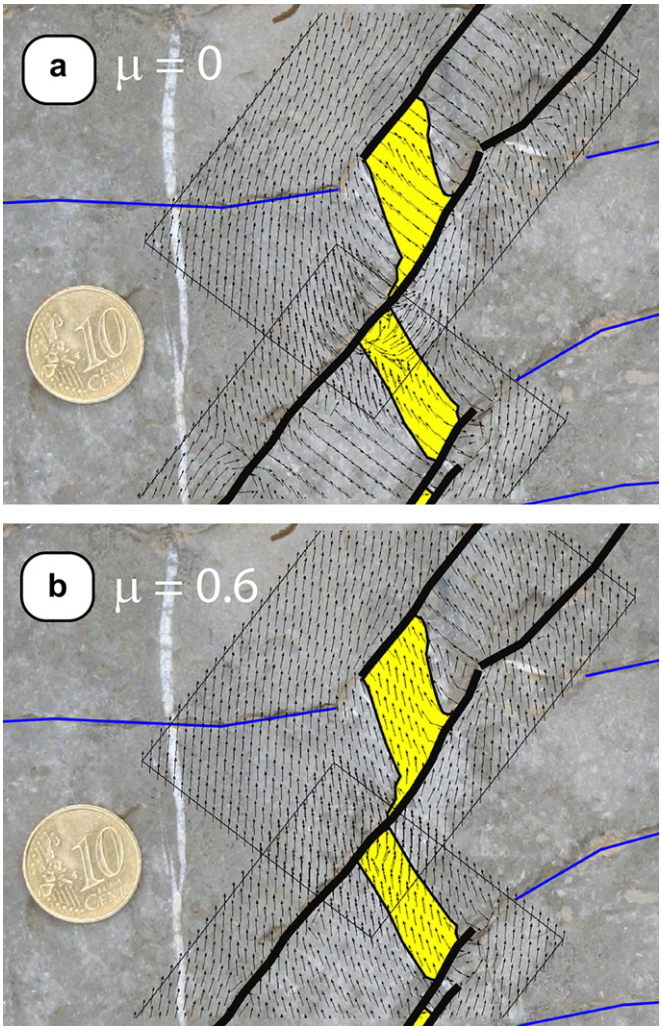


**Fig. 11.** Model results for the stylolites reactivated in shear shown in Fig. 9. (a) Model result for a $\mu = 0$. (b) Model result for a $\mu = 0.6$. The small arrows on the observation grid show the local orientation of $\sigma_1$.

approach is only suitable along faults if the remote stress conditions are well known, since the ratio of $\sigma_H/\sigma_h$ is very important for the stress orientation in the relay zone (Auzias, 1995). Any indicator of the remote and relay zone stress field are worth considering.

With regard to estimation of fault friction on large scale active faults, particular care must be taken with the stress field determined from data close to the Earth's surface. For depth shallower than 300 m, the orientation of the principal stress may be different than the tectonic stresses predominant at depth (e.g. Engelder, 1993). On large faults (kilometric scale length), it seems therefore more appropriate to provide an estimation of fault friction based on the tectonic stress orientation or the fracture patterns measured in deep bore holes, which are more representative of the brittle crust stress state.

This approach, based on field observation and numerical modeling at the relay zone, seems therefore relevant for the estimation of fault friction along active fault segments interacting through their stress field. Its main advantage compared to rock test measures, is the in situ estimation of the friction in its own geological context. We integrate a large part of the fault surface around the relay zone (and it can be done outside as well), as opposed to tests done on fault rocks, which correspond to a specific location of the fault surface crossed by the bore hole. Moreover, this approach provides an overall value of friction of the entire active fault zone, which may be composed of compartment with various fault rocks, as for example coarse cataclasites or gouges which can be difficult to analyse in laboratory tests. On the other hand, a limitation of this method is that permanent deformation (e.g. measured by GPS) can not be used to estimate friction with a quasi-static elastic model. Visco-elastic simulation of the lithosphere could be more appropriated if it allows to simulate the precise geometry of the fault segments.

## 6. Conclusion

In situ static friction can be estimated along a fault plane if its shape, the far field stress conditions and the stresses at its vicinity are well known. Joints and stylolites reactivated in shear show roughly different angles of linking fractures at their extensional relay zones. The irregular shape of the stylolites and the rectilinear trace of the joints suggest that different frictional behaviour may explain these differences in branching angles. Photoelastic and numerical modeling confirm this phenomenon. For the same remote stress conditions, variation of the static friction along simulated faults explains a wide part of the range of branching angle measured at relay zones. In particular, our paper reveals four main points:

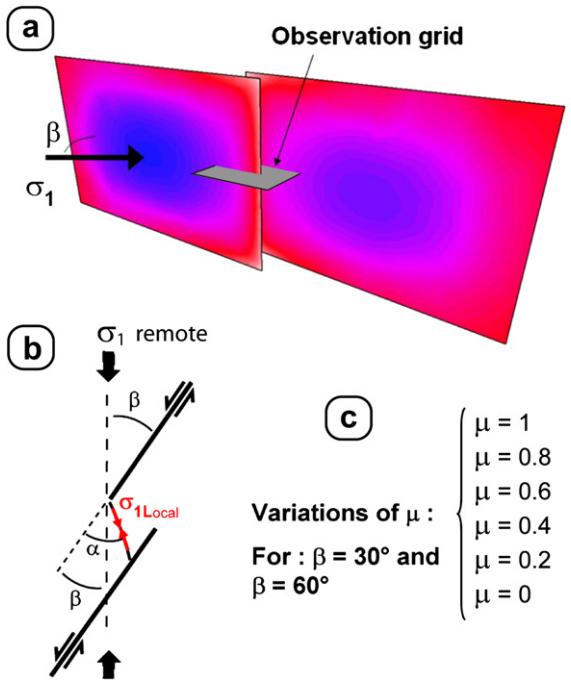


**Fig. 12.** Input conditions for the parametric modeling. (a) Configuration of the 3-D model geometry with an example of computed displacement contours in color. (b) Horizontal view of the model configuration showing the angles $\alpha$ and $\beta$. (c) Variables used in the parametric study.

(1) A simple Amonton's first law cannot be used systematically to infer the static friction along natural faults,
(2) To discuss the amount of friction along a fault, the analysis of the local stress field must be compared to elasto-static approaches that integrate the effect of mechanical interactions along ended faults, irregular in shape, segmented or more complex,
(3) Both field data, photoelasticity and numerical modeling show that wide variations of friction can explain a large part of the variation in the angle of secondary fracturing in the relay zones,

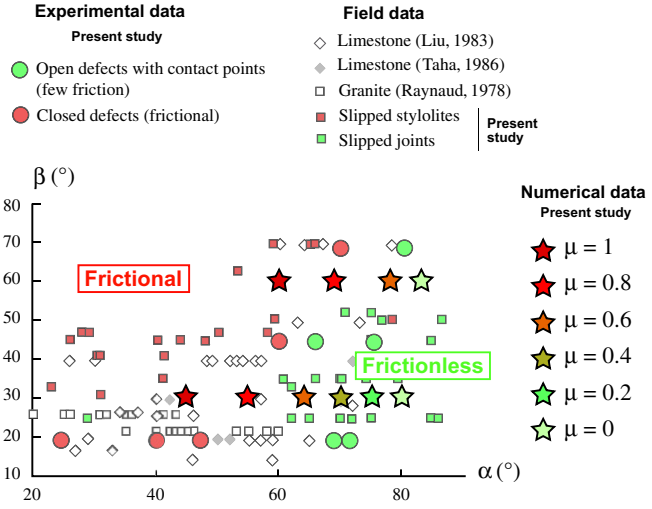


**Fig. 13.** Comparison of $\alpha$ and $\beta$ angles between the data obtained by numerical modeling, photoelastic modeling and the dataset measured in the field. A wide part of $\alpha$ and $\beta$ spreading can be explained by variations in frictional coefficient of the slipped defects.

(4) Shear-reactivated joints have lower estimated static friction than shear-reactivated stylolites.

## Acknowledgments

We which to particularly thank and dedicate this paper to Maurice Mattauer *who left us in April 2009*. He discovered the studied outcrop and recently participated to discussions about this work at the laboratory and also in the field. The field work from Roger Soliva was supported by an "Action Structurante 2006" grant from the laboratory Geosciences Montpellier UMR5243. W. Ashley Griffith and Roy Schlische are thanked for their helpful comments.

## References

d'Alessio, M.A., Blythe, A.E., Bürgmann, R., 2003. No frictional heat along the San Gabriel fault, California: evidence from fission-track thermochronology. Geology 31, 541–544.
Auzias, V., 1995. Photoelastic modeling of stress perturbations near faults and of the associated fracturing: petroleum industry application, II: Mechanism of 3D joint development in a natural reservoir analogue: the flat-lying Devonian Old Red Sandstone of Caithness (Scotland). Ph.D. thesis, Universite Montpellier II, p. 311.
Auzias, V., Rives, T., Rawnsley, K.D., Petit, J.-P., 1997. Fracture orientation modeling in the vicinity of a horizontal well. Bulletin Elf Aquitaine Production F64018, 381–397.
Barquins, M., Chaker, C., Petit, J.-P., 1997. Influence du frottement sur le branchement de fissures à partir de défauts obliques soumis à une compression uniaxiale. Compte Rendu de L'Academie des Sciences T324, 29–36.
Barquins, M., Petit, J.-P., 1992. Kinetic instabilities during the propagation of a branch crack: effects of loading conditions and internal pressure. Journal of Structural Geology 14, 893–903.
Barquins, M., Petit, J.-P., Maugis, D., Ghalayini, K., 1992. Path and kinetics of branching from defects under uniaxial and biaxial compressive loading. International Journal of Fracture 54, 139–163.
Bourne, S.J., Willemse, E.J.M., 2001. Elastic stress control on the pattern of tensile fracturing around a small fault network at Nash Point, UK. Journal of Structural Geology 23, 1753–1770.
Brace, W.F., Kohlstedt, D.L., 1980. Limits on lithospheric stress imposed by laboratory experiments. Journal of Geophysical Research 85, 6248–6252.
Brudy, M., Zoback, M.D., Fuchs, K., Rummel, F., Baumgartner, J., 1997. Estimate of the complete stress tensor to 8 km depth in the KTB scientific drill holes: implications for crustal strength. Journal of Geophysical Research 102, 18,453–18,475.
Brune, J.N., Henyey, T.L., Roy, R.F., 1969. Heat flow, stress, and rate of slip along the San Andreas fault, California. Journal of Geophysical Research 74, 3821–3827.
Bürgmann, R., Pollard, D.D., 1994. Strain accommodation about strike-slip fault discontinuities in granitic rock under brittle-to ductile conditions. Journal of Structural Geology 16, 1655–1674.
Byerlee, J.D., 1978. Friction of rocks. Pure and Applied Geophysics 116, 615–626.
Chaker, C., Barquins, M., 1996. Sliding effect on branch crack. Physics and Chemistry of the Earth 21, 319–323.
Comninou, M., Dundurs, J., 1975. The angular dislocation in a half space. Journal of Elasticity 5, 203–216.
Delair, J., Leroux, C., 1978. Méthodes de quantification de la disparition de matière au niveau de stylolites tectoniques et mécanismes de la deformation cassante des calcaires. Bulletin de la Société Géologique de France 7, 137–144.
Engelder, T., 1993. Stress Regimes in the Lithosphere. Princeton University Press, Princeton, New Jersey, U.S.A., 475 pp.
Fletcher, R.C., Pollard, D.D., 1981. Anticrack model for pressure solution surfaces. Geology 9, 419–424.
Hanks, T.C., 1977. Earthquake stress drops, ambient tectonic stress, and the stresses that drive plate motion. Pure and Applied Geophysics 115, 441–458.
Hatheway, A.W., Kiersch, G.A., 1989. Engineering properties of rock. In: Carmichael, R.S. (Ed.), Practical Handbook of Physical Properties of Rocks and Minerals. CRC Press, Boca Raton, FL, pp. 672–715.
Heténi, M., 1966. Handbook of Experimental Stress Analysis. Wiley, New York.
Joussineau, G., Petit, J.-P., Gauthier, B.D.M., 2003. Photoelastic and numerical investigation of stress distributions around fault models under biaxial compressive loading conditions. Tectonophysics 363, 19–43.
Kattenhorn, S.A., Aydin, A., Pollard, D.D., 2000. Joints at high angles to normal fault strike: an explanation using 3D numerical model of fault perturbated stress field. Journal of Structural Geology 22, 1–23.
Kattenhorn, S.A., Marshall, S.T., 2006. Fault-induced perturbed stress fields and associated tensile and compressive deformation at fault tips in the ice shell of Europa: implications for fault mechanics. Journal of Structural Geology 28 (12), 2204–2221.
King, G.C.P., Stein, R.S., Lin, J., 1994. Static stress changes and the triggering of earthquakes. Bulletin of the Seismological Society of America 84 (3), 935–953.
Lachenbruch, A., Sass, J., 1980. Heat flow and energetics of the San Andreas fault zone. Journal of Geophysical Research 85, 6185–6222.

Lovely, P.J., Pollard, D.D., Mutlu, O., 2009. Regions of reduced static stress drop near fault tips for large strike-slip earthquakes. Bulletin of the Seismological Society of America 99, 1691–1704.
Lunn, R.J., Willson, J.P., Shipton, Z.K., Moir, H., 2008. Simulating brittle fault growth from linkage of preexisting structures. Journal of Geophysical Research 113, B07403. doi:10.1029/2007JB005388.
Maerten, L., Gillepsie, P., Pollard, D.D., 2002. Effect of local stress perturbation on secondary fault development. Journal of Structural Geology 24, 145–153.
Maerten, F., Resor, P.G., Pollard, D.D., Maerten, L., 2005. Inverting for slip on three-dimensional fault surfaces using angular dislocations. Bulletin of the Seismological Society of America 95, 1654–1665.
Maerten, F., Maerten, L., Cooke, M., 2009. Solving 3D boundary element problems using constrained iterative approach. Computational Geosciences. doi:10.1007/s10596-009-9170-x.
Martel, S.J., 1997. Effects of cohesive zones on small faults and implications for secondary fracturing and fault trace geometry. Journal of Structural Geology 19, 835–847.
Moir, H., Lunn, R.J., Shipton, Z.K., Kirkpatrick, J.D., 2009. Simulating brittle fault evolution from networks of pre-existing joints within crystalline rock. Journal of Structural Geology. doi:10.1016/j.jsg.2009.08.016.
Mount, V., Suppe, J., 1987. State of stress near the San Andreas fault: implications for wrench tectonics. Geology 115, 1143–1146.
Mutlu, O., Pollard, D.D., 2008. On the patterns of wing cracks along an outcrop scale flaw: a numerical modeling approach using complementarity. Journal of Geophysical Research 113, B06403. doi:10.1029/2007JB005284.
Ohlmacher, G.C., Aydin, A., 1997. Mechanics of veins, fault and solution surface formation in the Appalachian valley, U.S.A.: implications for fault friction, state of stress and fluid pressure. Journal of Structural Geology 19, 927–944.
Okada, Y., 1985. Surface deformation due to shear and tensile faults in a half-space. Bulletin of the Seismological Society of America 75, 1135–1154.
Parsons, T., 2002. Nearly frictionless faulting from unclamping in long-term interaction models. Geology 30, 1063–1066.
Petit, J.-P., Barquins, M., 1988. Can natural faults propagate under mode II conditions? Tectonics 7, 1243–1256.
Petit, J.-P., Mattauer, M., 1995. Palaeostress superimposition deduced from mesoscale structures in limestone: the Matelles exposure, Languedoc, France. Journal of Structural Geology 17, 245–256.
Petit, J.P., Wibberley, C.A.J., Ruiz, G., 1999. 'Crack-seal, slip': a new fault valve mechanism? Journal of Structural Geology 21, 1199–1207.
Poliakov, A.N.B., Dmowska, R., Rice, J.R., 2002. Dynamic shear rupture interactions with fault bends and off-axis secondary faulting. Journal of Geophysical Research 107 no. B11, 2295. doi:10.1029/2001JB000572, ESE 6-1 6-18.
Rawnsley, K.D., Rives, T., Petit, J.P., Hencher, S.R., Lumsden, A.C., 1992. Joint development in perturbed stress fields near faults. Journal of Structural Geology 14, 939–951.
Raynaud, S., Carrio-Schaffhauser, E., 1992. Rock matrix structures in a zone influenced by a stylolite. Journal of Structural Geology 14, 973–980.
Rispoli, R., 1981. Stress fields about strike-slip faults inferred from stylolites and tension gashes. Tectonophysics 75, T29–T36.
Scholz, 2000. Evidence for a strong San Andreas fault.
Segall, P., Pollard, D.D., 1980. Mechanics of discontinuous faulting. Journal of Geophysical Research 85, 4337–4350.
Soliva, R., Benedicto, A., Maerten, L., 2006. Spacing and linkage of confined faults: the importance of mechanical thickness. Journal of Geophysical Research 111, B01402. doi:10.1029/2004JB003507.
Taha, M., 1986. Apport de la microtectonique cassante au problème des trajectoires de contraintes et de leurs perturbations. Exemples du Nord de Montpellier, thèse d'État, université de Montpellier, p. 155.
Thomas, A.L., 1993. Poly3d: a three-dimensional, polygonal element, displacement discontinuity boundary element computer program with applications to fractures, faults, and cavities in the earth's crust. Master thesis, Stanford University.
Wawersik, W.R., Brace, W.F., 1971. Post-failure behavior of a granite and diabase. Rock Mechanics 3, 61–85.
Willemse, E.J.M., 1997. Segmented normal faults: correspondence between three dimensional mechanical models and field data. Journal of Geophysical Research 102, 675–692.
Willemse, E.J.M., Pollard, D.D., 1998. On the orientation and patterns of wing cracks and solution surfaces at the tips of a sliding flaw or fault. Journal of Geophysical Research 103, 2427–2438.
Willson, J.P., Lunn, R.J., Shipton, Z.K., 2007. Simulating spatial and temporal evolution of multiple wing cracks around faults in crystalline basement rocks. Journal of Geophysical Research-Solid Earth 113 (2007). doi:10.1029/2007JB005388 B07403.
Zoback, M.D., Healy, J., 1984. Friction, faulting, and in situ stress. Annales Geophysicae 2, 689–698.
Zoback, M.L., Zoback, M.D., 1980. State of stress in the conterminous United States. Journal of Geophysical Research 85, 6113–6156.
Zoback, M.D., Zoback, M.L., Mount, V., Eaton, J., Healy, J., Oppenheimer, D., Reasonberg, P., Jones, L., Raleigh, B., Wong, I., Scotti, O., Wentworth, C., 1987. New evidence on the state of stress of the San Andreas fault system. Science 238, 1105–1111.
Zhou, X.P., 2006. Triaxial compressive behavior of rock with mesoscopic heterogenous behavior: strain energy density factor approach. Theoretical and Applied Fracture Mechanics 45, 46–63.